Growth and field emission properties of vertically aligned carbon nanofibers

C. H. P. Poa, S. J. Henley, G. Y. Chen, A. A. D. T. Adikaari, C. E. Giusca, and S. R. P. Silva[a)]
Nano-Electronics Centre, Advanced Technology Institute, University of Surrey, Guildford, GU2 7XH, United Kingdom

(Received 29 July 2004; accepted 8 March 2005; published online 24 May 2005)

Vertically aligned carbon nanofibers (VACNFs) were synthesized on Ni-coated Si substrates using a dc plasma-enhanced chemical-vapor deposition system. The size of the Ni islands used as catalyst to grow the VACNFs was formed by both thermal annealing and laser processing on thin metal layers. It was observed that the diameter of the carbon nanofibers is strongly dependent on the initial Ni island dimension. By varying the laser power from 228 to 279 mJ/cm^2, the size of these Ni islands can be controlled independent of the initial Ni film thickness. Electron field-emission results show that the emission threshold field is dependent on both the height and radius of these VACNFs and also field shielding effects. Threshold fields as low as 2 $V/\mu m$ was obtained from the sample with the largest height over radius ratio. © *2005 American Institute of Physics*.
[DOI: 10.1063/1.1899225]

I. INTRODUCTION

Carbon materials exist in a variety of forms and above all, carbon nanotubes (CNTs) have attracted the most interest in the last decade due to their unique properties. CNTs with high aspect ratio, good mechanical properties, and high current carrying capacity are especially suitable for tip-based electron field-emission devices. CNTs have promising field-emission properties and threshold fields as low as 1.6 $V/\mu m$ (for an emission current of about 1 nA) have been reported.[1] To obtain low threshold fields from field emitters, a large local electric field is required at the emitter's tip. The ratio of the local electric field over the applied geometrical macroscopic electric field is the field-enhancement factor β and is generally related to the height and radius of the emitter.[2] A possible approach to obtain high field-enhancement factors is to vertically align these CNTs perpendicular to the substrate. Since only the CNT tip is exposed to the anode, a high confinement of the electric field can be obtained hence increasing the local field at the tip. However, one drawback is when the CNTs are too closely packed together; the electric field is shielded away from neighboring CNTs.[3] To avoid such a problem, the separation distance between individual CNTs needs to be precisely controlled. The position, alignment, height, and tip radius of CNTs are controllable via the synthesis process.[4] CNTs and carbon nanofibers (CNFs), although originating from a similar catalyst, differ in terms of their diameter and structure. Generally speaking the CNT diameter is below 50 nm, with well-developed and aligned graphene planes parallel to the axis of growth in the nanotube. On the other hand, CNFs have a structure which is a mixture of aligned graphene planes as well as a bamboolike or cup-stacked structure, previously ascribed to herringbone-like structure. In general the fibers have a diameter in excess of 50 nm, and do not have a continuous void in the center of the tube. Their electrical properties also are more resistive due to the imperfect nature of the outer graphene planes.

Chemical-vapor deposition (CVD) techniques have been a popular choice for preparing CNTs. Thermal and plasma-enhanced CVD techniques are used to grow CNTs/CNFs over large areas by the decomposition of a suitable hydrocarbon gas over a transition-metal catalyst. Plasma-enhanced CVD (PECVD) has the advantage of producing VACNFs with much lower substrate temperatures than the thermal method.[4–6] Another advantage of using a CVD system is the ability of doping the CNT with gaseous dopants to enhance their conductivity. Commonly, the hydrocarbon gas is mixed with NH_3 in the deposition process to introduce the N dopant.[7,8] However, in the presence of a plasma, NH_3 becomes active in etching during deposition. In this work, we have synthesized nitrogenated VACNFs using dc plasma-enhanced CVD by the decomposition of C_2H_2 with N_2. This avoids the use of NH_3, which is a corrosive gas.

II. EXPERIMENT

The CNFs were synthesized using a dc-driven PECVD system with C_2H_2 as the hydrocarbon source and N_2 for dilution/doping purposes. The substrate table is heated using a graphite plate capable of reaching a temperature of 700 °C. The anode used in this system is a stainless-steel plate with a separation gap of 1.5 cm between the electrodes. The flow rate of the C_2H_2 and N_2 were fixed at 5 and 100 SCCM (denotes cubic centimeter per minute at STP), respectively, while the chamber pressure was maintained at 3–10 Torr. Ni thin films were thermally evaporated onto Si substrates which already had a thin layer of SiO_2. The SiO_2 was grown using thermal oxidation to a thickness of about 10 nm (according to ellipsometry measurements) and the Ni thin-film thickness is between 3 and 20 nm. Prior to deposition, the Ni thin films were first treated to thermal annealing at 700 °C in a nitrogen atmosphere (10 Torr) for 20 min for the formation

[a)]Electronic mail: s.silva@surrey.ac.uk

of nanosized islands which act as catalyst for CNF growth. C_2H_2 was introduced into the chamber when the bias applied between the electrodes was −500 V. Typically, deposition runs lasting 10 min were used to grow the CNF structures within our system.

A KrF Lambda Physik Excimer laser (LPX 210i) was also used for the nanostructuring of Ni. The laser operates at 248 nm with a pulse duration of 25 ns according to the manufacturer's specifications. The laser beam was homogenized and projected onto the Ni on Si using an aperture and optics. The pulse had a semi-Gaussian energy profile, 10 mm long, along the Gaussian direction, and 4 mm wide, along the constant energy direction. The nanostructuring was done in a chamber mounted on an X−Y stage, under a vacuum better than 1.33×10^{-2} Torr. The films were irradiated at a 10-Hz pulse repetition frequency and at 10 mm/s by means of scanning. This resulted in a pulse density of 10 per unit area. The best structures resulted at three specific Excimer energy fluences: 228, 264, and 279 mJ/cm^2.

The field-emission tests were carried out in a probe setup with a 5-mm diameter stainless-steel ball bearing as the anode. The anode can be moved is three directions where the gap between the anode and sample was varied in step sizes of 2.5 μm, driven by a stepper motor. The morphology and structures of the samples were investigated using scanning electron microscopy (SEM) and high-resolution transmission electron microscopy (TEM).

III. RESULTS AND DISCUSSION

Figure 1(a) shows the Ni thin film after annealing at 700 °C for 30 min. The initial Ni thickness was 4.5 nm, prepared by thermal evaporation of a Ni wire. The formation of nanosized islands is due to the heat applied to the sample which causes the thin film to sinter due to surface tension. Figure 1(b) shows the size distribution of the sample fitted to a log normal function giving a mean particle size of 125 nm and a standard deviation of 62 nm. It can be observed that using this technique the islands formed are generally irregular and the standard deviation is large. The average island size is about 16 times the original film thickness. SEM images of samples with different island sizes of 34, 69, 140, and 180 nm are shown in Figs. 2(a)–2(d), respectively. These correspond to the initial Ni film thicknesses of 2.5, 3, 4.5, and 6.7 nm, respectively. The nanofibers grown from these substrates are shown in Figs. 2(e)–2(h). These VACNFs were synthesized at 700 °C with a 100:5 gas ratio of $N_2:C_2H_2$ and cathodes biased at −450 V. The process pressure was kept at 3.6 Torr for the 10 min duration of the growth.

The variation of the initial Ni film thickness to the island size is shown in Fig. 3(a). This is in agreement with the work of Nerushev *et al.*[9] and Chhowalla *et al.*[4] where the island size increases with thicker Ni films. Also in agreement with Ref. 4, the shape of these Ni islands is irregular. The dimensions of these islands are important as they act as the catalyst for nanotube synthesis and controls the CNF diameter. The variation of the CNF diameter with the Ni island size is shown in Fig. 3(b). It is interesting to note the CNF diameter is proportional to the island size multiplied by a factor of 0.8,

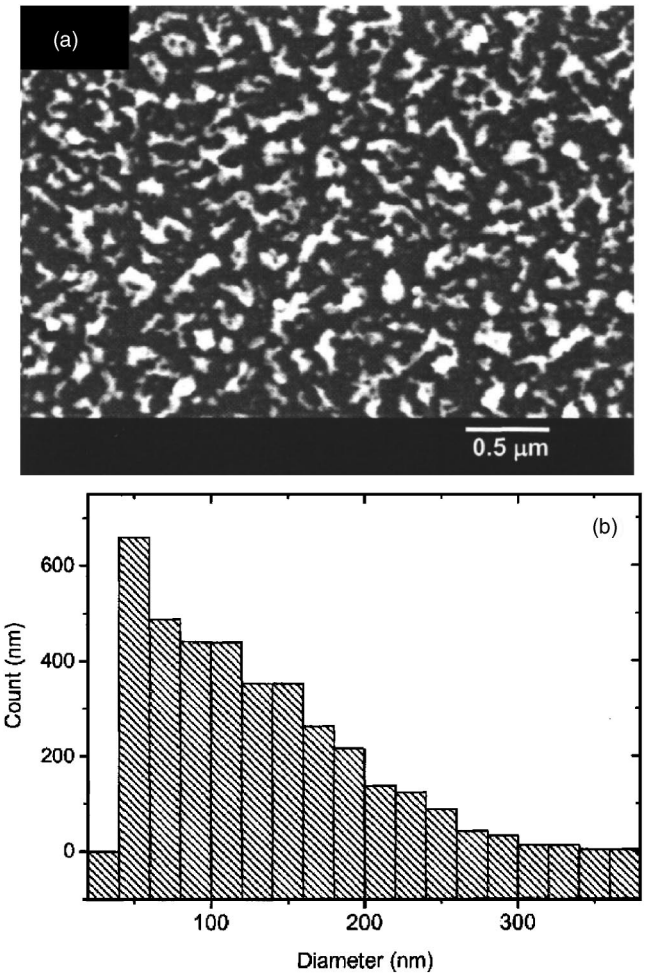

FIG. 1. (a) SEM image of the thermally annealed Ni film with an initial thickness of 4.5 nm. (b) Distribution of the Ni islands with a mean size of 125 nm and standard deviation of 62 nm according to the analysis of the above SEM micrograph.

which indicates that during the growth process, the Ni islands have been deformed or contracted. This reshaping of the Ni nanoparticle is due to the nucleation and growth of graphene layers around it. This process creates restructured monoatomic step edges at the nickel surface during C–Ni diffusion.[10]

Control of the Ni island dimension is crucial in producing CNFs that are uniform in dimension. Thus far, the only way of controlling the island size is via the Ni thin-film's initial thickness.[4] Also the irregular shape of the Ni island

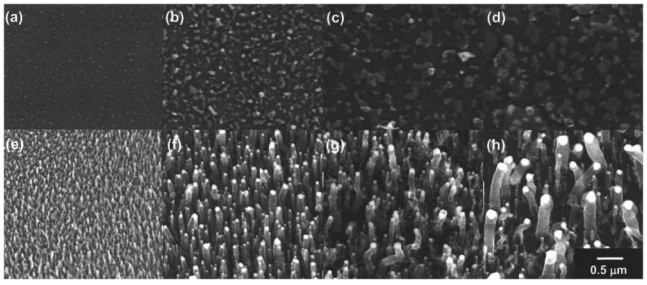

FIG. 2. (a)–(d) Show SEM images of films with different island sizes of 34, 69, 140, and 180 nm, respectively. Nanofibers grown from these substrates are shown in (e)–(h).

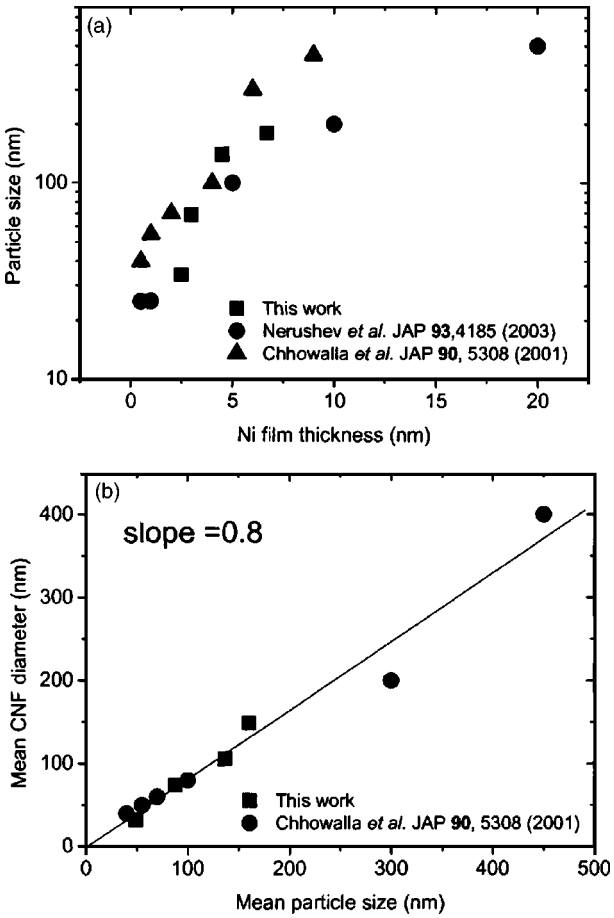

FIG. 3. (a) Variation of the particle size as a function of the initial Ni thickness. (b) Variation of the mean CNF diameter as a function of the mean particle size.

may result in more than one CNF growing from a single island.[11] In this work, we employed a laser system to modify the Ni islands via laser annealing. At high energy (>279 mJ/cm^2), the Ni can be completely sputtered off the substrate. Figures 4(a)–4(c) show the SEM images of the Ni film (initial thickness of 4.5 nm) laser annealed at 228, 264, and 279 mJ/cm^2, respectively. The CNF synthesized from the same series is shown in Figs. 4(d)–4(f). The laser-annealed film at 228 mJ/cm^2 is shown in Fig. 4(a). Upon annealing, the Ni film breaks up into droplets that are more

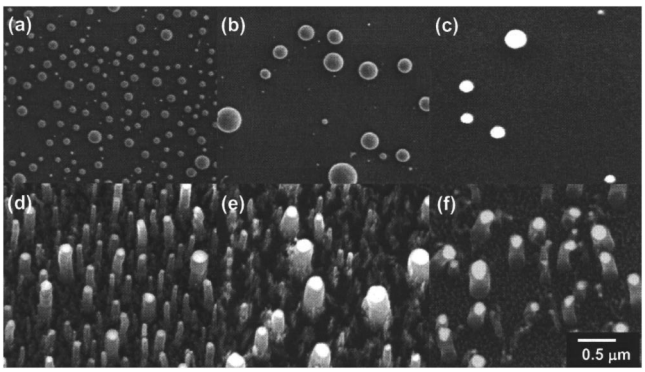

FIG. 4. (a)–(c) SEM images of Ni droplets formed by laser annealing at 228, 264, and 279 mJ/cm^2, respectively. (d)–(f) Show the CNF synthesized from the same series (initial thickness of 4.5 nm).

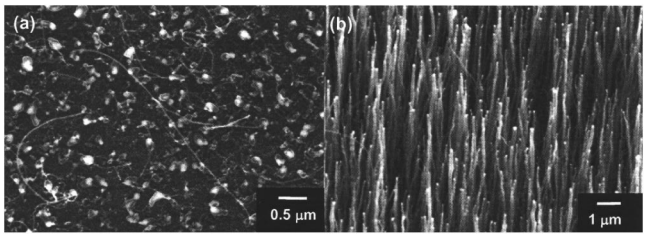

FIG. 5. CNFs grown using (a) thermal CVD and (b) PECVD techniques, with gases of C_2H_2 and N_2 at 700° C at a pressure of 10 Torr.

spherical in shape as compared to the sample that is heat treated. These droplets have a more uniform distribution and smaller standard deviation. However, after CNF synthesis there are smaller CNFs (undergrowth) observed despite the Ni islands not being visible before growth. As the laser energy increases, the mean Ni island size increases. It is interesting to note that this technique produces larger islands than those that are thermally annealed. Also in Figs. 3(d) and 3(e) there are undergrowths of nanofibers present. It can be seen that at high energy [Fig. 4(f)] only large Ni islands are present after laser processing. The CNF has a diameter of about 175 nm and the undergrowth is no longer present. Using this technique, we are able to control the size of the Ni islands despite having the same initial Ni film thickness and also the interseparation distance between individual islands is more spacious than the thermally prepared samples. This separation is important as the electric-field shielding effect[3] during electron field emission can be minimized.

Figures 5(a) and 5(b) show the difference between a thermal CVD and a PECVD-grown CNF. Both samples were grown at 700 °C for 20 min with a N_2:C_2H_2 ratio of 100:5 at 10 Torr process pressure. The sample in Fig. 5(b) is synthesized with PECVD at a cathode bias of −450 V. It can be seen that if no plasma is present, the CNFs are curly and nonaligned. However, in Fig. 5(b) the tubes are more uniformly grown and vertically aligned to the substrate. This sample is believed to be a much better field emitter since there are more tips exposed to the surface. Thus far, the mechanism for the aligning of these tubes is not completely understood. However, vertical alignment due to "crowding" of CNTs (Ref. 12) and preferential plasma etching seems to be unlikely.[13] Instead, we believed that the alignment is due to the electric field in the plasma sheath region, which is in agreement with the work in Ref. 4.

Figure 6 shows the effect of plasma-enhanced deposition. The process pressure and deposition rate has been lowered to reduce the growth rate of CNFs so that the effect of the plasma can be clearly observed. These samples were synthesized at 3.6 Torr for 10 min but with varying the cathode bias from 0 to −500 V. Figure 6(a) shows the as-prepared Ni islands before deposition. Figures 6(b)–6(f) represent a bias from −300, −350, −400, −450 and −500 V, respectively. By increasing the dc bias, the growth rate increases and also at −500 V the CNFs are much better aligned. By introducing a plasma, it is believed that the local temperature at the growing CNF increases and hence creating a temperature gradient. This model is in agreement with the model proposed by Baker *et al.*[14]

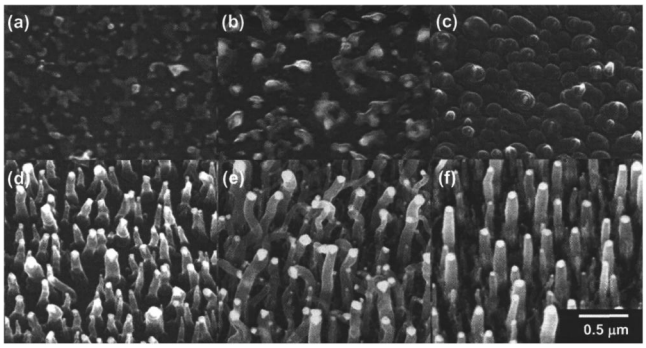

FIG. 6. SEM images of CNF growth as a function of the dc bias for (a) the substrate before growth, (b) at −300 V with no plasma, (c) −350 V, (d) −400 V, (e) −450 V, and (f) −500 V.

Electron field-emission characterization was carried out is a scanning probe setup. A voltage of 0–2000 V is applied between the CNF sample (cathode) and the stainless-steel ball bearing anode over a separation gap of 50–150μm. Therefore, the CNF lengths becomes negligible in comparison to the vacuum gap. The applied electric field is a division of the applied voltage over the separation gap. Here, the gap is obtained by controlling the stepper motor attached to the probe. The threshold field (E_{th}) is defined as the applied electric field required for an emission current of 1 nA.

Figure 7 shows the field-emission characteristics of the aligned and nonaligned CNFs and the SEM images of these samples are shown in Figs. 5(a) and 5(b). The emission current remains in the range of 1×10^{-10} A, before increasing in an exponential manner with respect to the applied field. The emission current is limited to a value of 10 μA to prevent a sudden surge of current in the system. The E_{th} for the vertically aligned CNF is about 2 and 4.5 V/μm for the nonaligned sample. Since the VACNF has more tips exposed to the anode, one would expect that E_{th} would be much lower than the nonaligned one. This can be explained by the electric-field screening effect that has been described previously by Nilsson *et al.*[3] The neighboring CNT shields away the electric field from the surrounding, and therefore reducing the local field at the tip. It has been proposed that in order to obtain a maximum field enhancement, the separation between each CNT has to be twice the height of the CNT.[3] As for the nonaligned CNT, the emission is mainly dominated by those that are much longer than the surrounding. One would expect that the emission site density will be different, and the VACNF would have a higher number of emission sites.

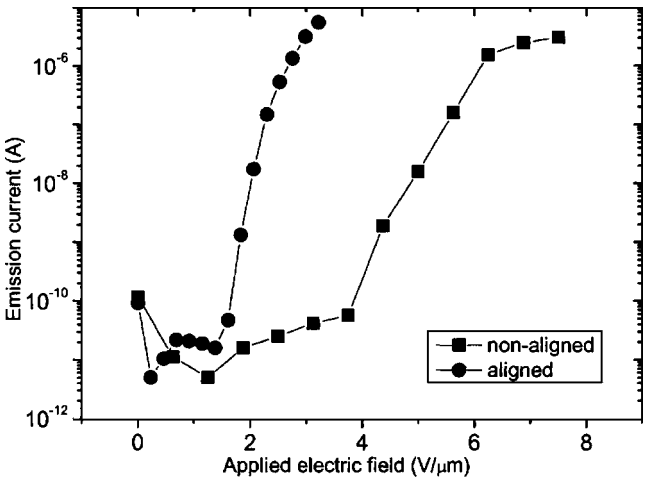

FIG. 7. Field-emission characteristics of nonaligned and vertically aligned CNF samples.

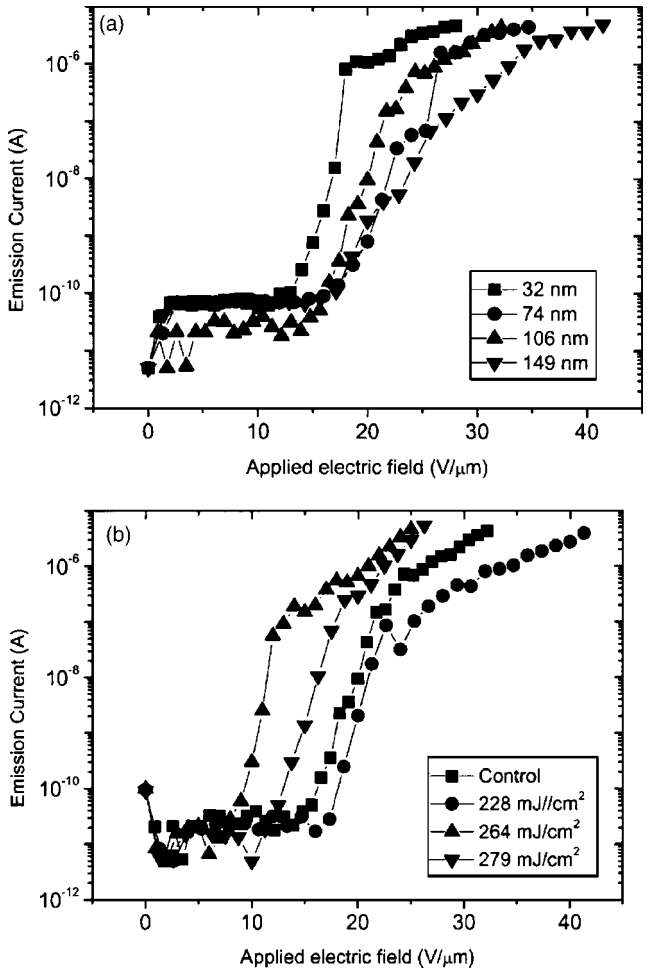

FIG. 8. Field-emission characteristics (a) as a function of different CNF diameters and (b) of CNFs where catalysts were laser annealed.

Figure 8(a) shows the field-emission characteristics of those samples shown in Figs. 2(e)–2(h). There are no significant differences between these samples in terms of E_{th} which is between 16 and 21 V/μm. The lowest E_{th} is observed from the film with the smallest CNFs. Compared to the E_{th} on Fig. 7, these E_{th} are much higher since the CNFs are much shorter. The emission threshold field is related to the local field experienced by the emitter. To increase the local field, one can increase the aspect ratio of the emitter which is related to its height and radius. However, these samples are intentionally grown shorter so that these effects can be easily observed. The field-emission results from the samples that have been laser annealed are more complicated. Figure 8(b) shows the field-emission characteristics of these samples that have been annealed at 228, 264, and 279 mJ/cm^2 prior to CNF growth and the control has the Ni island thermally annealed. For the sample that is annealed at 228 mJ/cm^2 there is no significant difference in E_{th} compared to the control

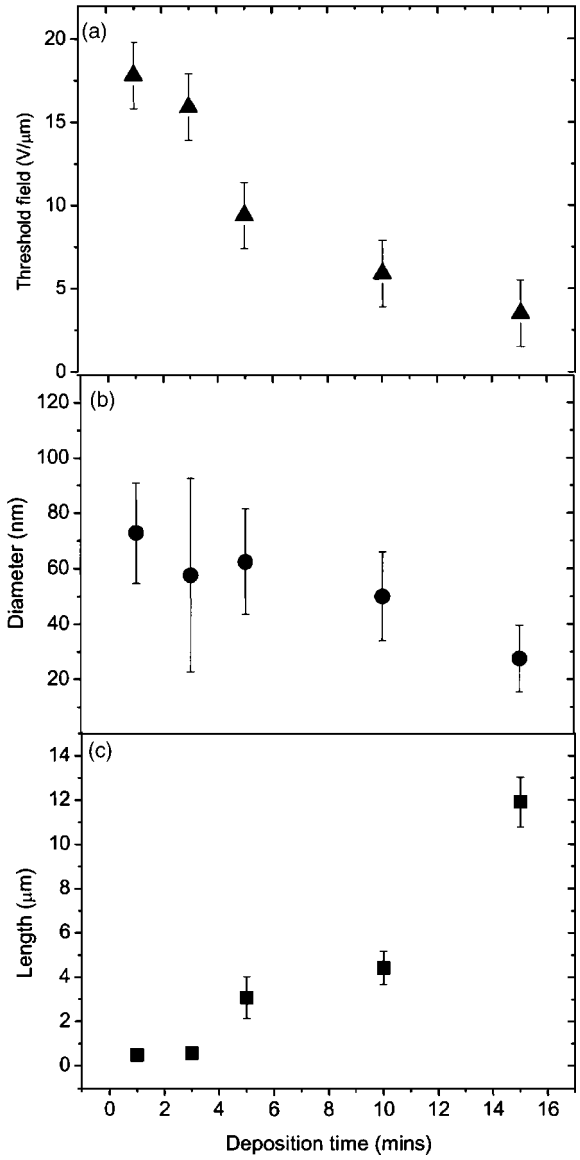

FIG. 9. (a) Field-emission threshold field, (b) CNF tip diameter, and (c) CNF length as a function of deposition time. These CNFs are grown with gases of C_2H_2 and N_2 at 700° C at a pressure of 10 Torr.

sample. Increasing the laser energy further to 264 mJ/cm^2 has created smaller Ni islands as undergrowths in addition to the larger diameter fibers. These smaller diameter CNF undergrowth decreases in the threshold field from 15 to 11 $V/\mu m$. For further increase in laser energy E_{th} increases to 14 $V/\mu m$ with the CNFs being much larger than the control sample. It is possible that the electric-field screening effect is minimized due to spacing of the CNFs.

In order to investigate the effects of tube aspect ratio, CNFs were grown as a function of different synthesis times of 1–15 min while keeping other conditions constant. Figure 9 shows the (a) field-emission (FE) threshold field, (b) CNF tip diameter, and (c) CNF length as a function of deposition time. It is important to note that each FE threshold field is an average of five different FE measurements on the sample while the dimensions of the CNFs were obtained from their statistical distribution over a sampling of 50 CNFs in each case. It can be seen from Fig. 9(c) that the height of the

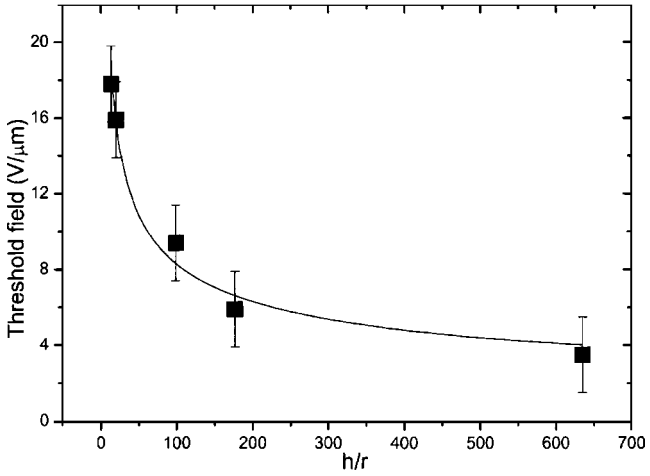

FIG. 10. Field-emission threshold fields as a function of h/r. The value of h/r is a geometrical factor of the CNF and is proportional to β. The curve is fitted to a function of $y=ax^b$ where a is a constant and we obtained $b=-0.4$.

CNFs increases with deposition time. The growth rate is nonlinear and we attribute this to the retardation effect from the Ni particles during the initial growth process. With reference to the tip growth model, the initial growth process includes the uplifting and deformation of the Ni islands and therefore reducing the growth rate between the 1- and 5-min syntheses. Another piece of evidence for the deformation of the Ni particle can be seen from Fig. 9(b), where the diameter of the CNF tip decreases as the CNF length increases. It is interesting to note that the initial diameter of the Ni islands is about 125 nm, while the CNF tip diameter decreases from 72 to 27 nm for the 1–15 min deposition time, respectively. The FE threshold field as a function of the deposition time is shown in Fig. 9(a). The threshold fields for electron emission decreases from 18 to 3 $V/\mu m$ as the height of the CNF increases and the diameter decreases. This shows that the field enhancement during the FE process is dependent on the geometrical effect of the CNF/CNT. This enhancement factor β is roughly proportional to the factor of h/r, where h and r are the height and radius of the emitter, respectively. Figure 10 shows the threshold fields as a function of the h/r factor extracted from the data in Fig. 9. Interestingly, the threshold field is proportional to h/r by a power law of -0.4; this relationship suggests that the effect of electric-field screening gets stronger and reduces β as the length of the CNF increases.

The field-emission results presented thus far have been emphasized as being applicable over large areas. Since carbon nanotubes are generally very small as compared to the large probe measurements (5-mm diameter), the emission current can be dominated by only a few nanotubes, especially in the nonaligned sample. In order to probe the FE characteristics in a microscopic scale, we modified a SEM system to perform scanning field-emission measurements. The samples were mounted on an electrically isolated specimen stage in a Cambridge Instruments Stereoscan scanning electron microscope. The electron field-emission anode is a tungsten wire sharpened via electrochemical etching, with tip radius of less than 500 nm. The tip can be moved within the

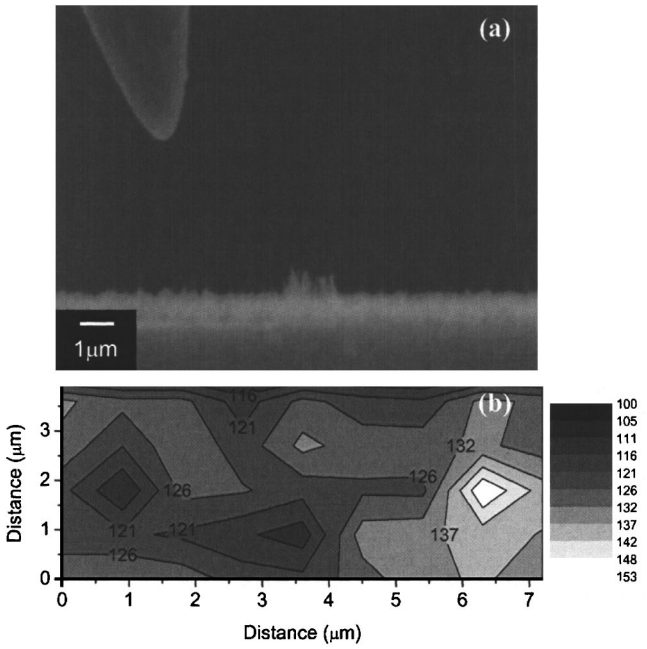

FIG. 11. (a) SEM image of the experimental setup where the probe is set 3 μm above the sample and scanned across an area of 4×7.2 μm. The CNF length is about 1.2 μm with a radius of 30 nm. (b) The 3D contour map of the threshold fields across the sample. The contour scale on the right represents the variation of the threshold field in V/μm. (The threshold field is defined as the applied electric field when an emission current of 1 nA is observed.)

SEM, independent of the stage, by three piezosliders (Omicron Nanotechnology, MS5), with a minimum step size of 40 nm, and up to 5-mm total travel. Figure 11(a) shows the SEM image of the experiment with the probe suspended above the CNF film. The probe is kept at 3 μm above the surface of the sample and field-emission characteristics were measured as the probe was scanned across the sample with an area of 7.2×4 μm at a step size of 400 nm. The results were then analyzed and the threshold fields for the emission current of 1 nA plotted in a three-dimensional (3D) contour plot shown in Fig. 11(b). It can bee seen that the threshold fields are not uniform across the sample surface and can be correlated to the surface features observed in the SEM image. The threshold fields vary from 156 to 108 V/μm, which is much higher that the value observed in the larger probe measurements 18 V/μm. There are two reasons for the discrepancy in this case: (1) the emission area is smaller and more localized, and (2) the emission current is generally contributed by a few tubes which are suppressed by the proximity effect. When we compare the surface morphology from the SEM image to the FE results, it can be seen that protruding tubes dominated the FE current when probed locally. The 3D contour map shows that the microscopic FE characteristics need to be interpreted very differently as the field-enhancement factor and local electric field are different in a macroscopic measurement.

IV. SUMMARY AND CONCLUSIONS

In summary, we have examined the growth of CNFs from different initial Ni catalyst island configurations prepared using a number of techniques. The Ni island is shown to be directly related to the CNF diameter and can be controlled by changing the initial Ni film thickness or laser annealing condition for the thin film with different laser energy densities. The structures observed in the SEM show that the growth mechanism is based on a tip growth model and the nanofibers are defective in the body of the tubes due to the effect of the Ni catalyst moving upwards toward the anode during growth.

The field-emission results show that E_{th} is dependent on the height and radius of the nanofibers. However, by varying the spacing between individual tubes there is a reduction in the threshold field that is due to lowering of the electric-field screening, despite the increase in tip radius giving rise to lower β values.

ACKNOWLEDGMENT

The authors would like to acknowledge the financial support received from the EPSRC Carbon Based Electronics Programme and Portfolio Partnership Award.

[1]C. H. Poa, S. R. P. Silva, P. C. P. Watts, W. K. Hsu, H. W. Kroto, and D. R. M. Walton, Appl. Phys. Lett. **80**, 3189 (2002).
[2]I.-M. Bonard, K. A. Dean, B. F. Coll, and C. Klinke, Phys. Rev. Lett. **89**, 197602 (2002).
[3]L. Nilsson, O. Groening, C. Emmenegger, O. Kuettel, E. Schaller, and L. Schlapbach, Appl. Phys. Lett. **76**, 2071 (2000).
[4]M. Chhowalla *et al.*, J. Appl. Phys. **90**, 5308 (2000).
[5]B. O. Boskovic, V. Stolojan, R. U. A. Khan, S. Haq, and S. R. P. Silva, Nat. Mater. **1**, 165 (2002).
[6]S. Hofmann, C. Ducati, J. Robertson, and B. Kleinsorge, Appl. Phys. Lett. **83**, 135 (2003).
[7]W.-Q. Han *et al.*, Appl. Phys. Lett. **77**, 1807 (2000).
[8]C. J. Lee, S. C. Lyu, H.-W. Kim, J. H. Lee, and K. I. Cho, Chem. Phys. Lett. **359**, 115 (2002).
[9]O. A. Nerushev, S. Dittmar, R.-E. Morjan, F. Rohmund, and E. E. B. Campbell, J. Appl. Phys. **93**, 4185 (2003).
[10]S. Helveg, C. Lopez-Cartes, J. Sehested, P. L. Hansen, B. S. Clausen, J. R. Rostrup-Nielsen, F. Abild-Pedersen, and J. K. Nørskov, Nature (London) **427**, 426 (2004).
[11]K. B. K. Teo *et al.*, Nanotechnology **14**, 204 (2003).
[12]S. Fan, M. G. Chapline, N. R. Franklin, T. W. Tombler, A. M. Cassell, and H. Dai, Science **283**, 512 (1999).
[13]V. I. Merkulov, D. H. Lowndes, Y. Y. Wei, G. Eres, and E. Voelkl, Appl. Phys. Lett. **76**, 3555 (2000).
[14]R. T. K. Baker, P. S. Harris, R. B. Thomas, and R. J. Waite, J. Catal. **30**, 86 (1973).